Crystallization, Mechanical, and Rheological Behavior of Polyvinylidene Fluoride/Carbon Nanofiber Composites

Shailesh Vidhate,[1] Ali Shaito,[1] Jaycee Chung,[2] Nandika Anne D'Souza[1]

[1]*Department of Materials Science and Engineering, University of North Texas, Texas 76203*
[2]*Global Contour Ltd., Rockwall, Texas*

Received 20 May 2008; accepted 29 September 2008
DOI 10.1002/app.29413
Published online 22 December 2008 in Wiley InterScience (www.interscience.wiley.com).

ABSTRACT: Composites of polyvinylidene fluoride (PVDF)/carbon nanofibers (CNFs) with different nanofiber contents were prepared by melt-blending using a twin-screw extruder by directly mixing CNFs with PVDF in the molten state. Fibers were extruded from the blended pellets. CNFs improved the nucleation efficiency of PVDF but the percent crystallinity decreased with increasing CNF concentration. X-ray diffraction results showed a change in the α phase, but the transition to the β phase did not occur. Dynamic mechanical analysis (DMA) indicated an improvement in storage modulus and reduced damping factor with increasing CNF concentration. A complementary improvement in mechanical properties was determined from tensile test results. Rheological measurements indicated increased storage modulus, loss modulus, and viscosity values with an increased percentage of CNFs in the PVDF. © 2008 Wiley Periodicals, Inc. J Appl Polym Sci 112: 254–260, 2009

Key words: polyvinylidene fluoride; carbon nanofibers; crystallization; fibers; dynamic mechanical analysis

INTRODUCTION

Reinforcement of polymers by carbon-based nanofillers has been of increasing interest because of the multifunctional properties that they result in. Polyvinylidene fluoride (PVDF) has attracted interest because it is a piezoelectric, pyroelectric, and ferroelectric material.[1–4] PVDF is a semicrystalline polymer with a high molecular weight and typically has around 50% amorphous content. PVDF shows various interesting properties like ease of processability, good mechanical properties, thermal stability, and chemical resistance.[5] Five crystal structures are present in PVDF. The electrical properties have been correlated to the β phase, which has been found to induce polarity in the crystal structure. When PVDF is uniaxially oriented, it results in longitudinal deformation of polymer chains in the crystals and increased β-phase formation.[6] Nunes et al.[7] have shown that the α phase can be converted into β phase by mechanical stretching below 100°C using a stretch ratio of about 3–5, or directly from solution at a given temperature. Some researchers have processed PVDF into porous and nonporous films that have had a 100% β phase.[8–10]

Correspondence to: N. A. D'Souza (ndsouza@unt.edu).
Contract grant sponsor: Global Contour Ltd.

PVDF with nanofillers like carbon nanotubes (CNTs), carbon black, and calcium carbonate has been widely studied. The concept of nanoreinforcement is based on the fact that a low percentage (3–5%) of loading can result in a major change in the properties of polymers. Mechanical properties, thermal conductivity, electrical conductivity, flame retardance, and wear resistance have all shown benefits from nanofillers.[11] Single-walled CNT (SWCNT) and PVDF composites have demonstrated an increase in mechanical, conducting, and ferromagnetic properties.[12] Yu et al.[13] showed that montmorillonite clays act as nucleating agent and cause the formation of a γ phase. For clay content greater than 1 wt %, α and β phases coexist.[13] When multiwalled CNTs (MWCNTs) are incorporated, the crystallites are transformed from the nonpolar α form to polar β form. A percolation threshold for electrical and thermal conductivity was observed at 2–2.5 wt % of MWCNT.[14,15] MWCNTs also offer ease of processing, flexibility, and good dielectric behavior of PVDF film.[16,17] CNT-filled PVDF thin films indicated an excellent acoustic response, acting as a transducer over a broadband frequency range. In addition, the films were transparent (invisible sound monitors for military applications), flexible, and lightweight.[18] Among the various nanofillers, an increase in electrical conductivity was also observed with the addition of carbon black.[19] Vapor-grown carbon fibers (VGCFs) have been attracting much research interest as fillers in composites because of their good

electrical, thermal conductivity, and mechanical properties.[20] There is to date limited information on carbon nanofiber (CNF) reinforcement of PVDF, to our knowledge. However, cost comparisons of MWCNTs, SWCNTs, and CNFs indicate that CNFs remain very cost-competitive. The purpose of this study is to investigate the effects of CNFs on the thermal, mechanical, and rheological properties of PVDF at different weight percentage loadings.

EXPERIMENTAL

Materials

The PVDF used was supplied by Arkema (Kynar® 721, powder form) and had the following properties:

- Density: 1.78 g/cc.
- Melt flow index (MFI): 10 g/10 min.
- Tensile strength: 54 MPa.
- Melting temperature: 168°C.

CNFs were obtained from Pyrograf® Products. (PR-24-XT-LHT), with the following material properties:

- Bulk density: 1.95 g/cc (ASTM D1513-86).
- Average diameter: 107 nm (JEOL 5300 SEM).

CNFs were used as received without further purification. Prior to melt-mixing, both the materials were vacuum-dried at 80°C for 6 h. PVDF and CNFs were dry-mixed via tumbling in a bottle. The contents of CNFs in PVDF powder were 0, 1, 2, and 4 wt %; and the compositions were coded as PVDF, PVDF1, PVDF2, and PVDF4, respectively.

Preparation of PVDF fibers

Melt-blending of PVDF and CNFs was performed in a twin-screw corotating extruder. The extruder temperatures were set from 170°C at the feed zone to 210°C at metering zone. Screw rpm was 200. Substantial shear forces are necessary during the composite processing step to disperse nanofibers in the polymer and to achieve good mechanical and electrical properties.[21] Fiber pulling roll speed was set to 230 rpm to ensure mechanical stretching of fibers, which is anticipated to lead to orientation of CNFs and polymer crystallites in the direction of the pulling.[22] Extruded fibers with an average diameter of 0.5 mm were obtained in product form.

Differential scanning calorimetry

The crystallization and melting behavior of PVDF/CNF compositions were investigated by using the Perkin–Elmer DSC 6 in a nitrogen atmosphere. Approximately 4–6 mg of sample was sealed in an aluminum pan. Heating and cooling scans was performed at 10°C/min between 30 and 220°C. Samples were held at 220°C in the molten state for 5 min to eliminate previous thermal history prior to cooling scan.

X-ray diffraction

The crystal structure of PVDF and composites were studied by wide-angle X-ray diffraction (WAXD). The diffraction patterns were obtained with a Rigaku Ultima III using CuKα radiation with a wavelength of 0.154 nm at 40 kV and 100 mA. Measurements were made between 2θ values of 2° and 40° with a scan speed of 2°/min.

Mechanical testing

Tensile tests were carried out on the extruded fiber samples with a TA Instruments RDS III DMA in the tensile mode. The shapes of the samples were cylindrical with 50 mm gauge length and 0.5 mm diameter. The crosshead speed was set at 5 mm/min. For each data point, three samples were tested, and the average value was taken.

Dynamic mechanical measurements

DMA was conducted on a TA Instruments RDS III under nitrogen using a heating rate of 3°C/min and a frequency of 1 Hz between −100 and 120°C. A fiber sample with a 0.5 mm diameter and 40 mm length was used.

Scanning electron microscopy

A high resolution SEM (FEI Nova 200 Dual Beam FIB/FEGSEM) was used to observe the dispersion of CNF in the PVDF matrix. The samples were dipped in liquid nitrogen for 3 min and fractured. Gold coating was done on the fractured surface to avoid overcharging of polymeric samples during SEM imaging. The gold-coated surface was imaged using beam of 1.7 nA at 5 kV of accelerating voltage.

Melt rheology

Rheological measurements were carried out on a TA Instrument's ARES strain-controlled rheometer. For the rheological study, a 25-mm parallel plate setup was used. Extruded fibers were used to prepare rheological disc samples having a diameter of 25 mm and a thickness of 2.5 mm in a compression press at 180°C. Dynamic strain sweep measurements were carried out at a frequency of 1 Hz, a

temperature of 180°C, and a strain of 0.1–100% to determine the linear viscoelastic region. The gap between the two parallel plates was 0.051 mm.

RESULTS AND DISCUSSION

Crystallization behavior

DSC results of the pure PVDF and composites are summarized in Table I. Melting temperature (T_m), melting enthalpy (ΔH_m), crystallization temperature (T_{mc}), melt crystallization temperature (T_{mc}), and melt crystallization enthalpy (ΔH_{mc}) were obtained from the second-heating and second-cooling thermograms.

Figure 1 shows the DSC second-heating curves for all compositions. PVDF has a melting temperature of 168°C and a melting enthalpy of 58.08 J/g. For low-filler compositions (PVDF1 and PVDF2), no significant change in melting point was observed; but melting enthalpies (ΔH_m) dropped to 41.29 and 31.56 J/g. A high-filler loading of 4% resulted in a significant increase in melting to 170°C, but enthalpy remained lower than the pure PVDF but a little higher than PVDF3 (42.03 J/g).

Figure 2 shows the DSC second-cooling curves. The crystallization point for all the compositions increased for all composites relative to that of pure PVDF. The crystallization temperature increased with the increase in CNF content. The crystallization temperatures (T_{mc}) of PVDF and composition PVDF4 are 138.4 and 145.25°C, respectively. These temperatures show that CNFs act as nucleating agents for PVDF. The corresponding degree of crystallinity (X_c) was determined by

$$X_c = [\Delta H_c/\Delta H_0] \times X_m \times 100\%,$$

where ΔH_0 is the enthalpy of 100% crystalline PVDF (105 J/g),[23] and X_m is the weight fraction of PVDF in the composite. The degree of crystallinity was found to be 60, 50, 38, and 47% for PVDF, PVDF1, PVDF2, PVDF4, respectively. The trends complement the results of the heating scan and the tendency for the enthalpy to drop with concentration for PVDF1 and PVDF2 but to increase for PVDF4 is once again

TABLE I
DSC Results from Second-Heating and Second-Cooling Thermograms

Sample ID	T_m (°C)	ΔH_m (J/g of PVDF)	T_{mc}	ΔH_{mc} (J/g)	X_c (%)
PVDF	168	58.081	138	−62.625	55.32
PVDF1	168	41.298	141	−52.068	39.33
PVDF2	168	31.568	144	−40.455	30.06
PVDF4	170	42.0395	145	−50.288	40.04

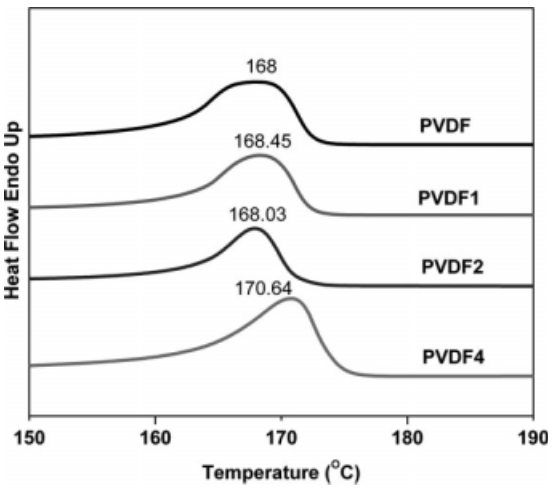

Figure 1 DSC second-heating curves showing an increase in melting point with increasing CNF content.

observed. Although the CNF enhanced the nucleation efficiency of the PVDF, the crystallinity decreased with increasing concentration. With an unchanged melting point but increased recrystallization temperature, the difference between melting and recrystallization temperatures decreased. This indicates a reduced degree of supercooling in the composites with the presence of CNF. The glass transition of PVDF was undetected by DSC.

Dynamic mechanical behavior

DMA was used to determine the dynamic mechanical properties of the samples in which the sample is subjected to repeated small-amplitude strains in a cyclic manner. The DMA T_g was found by examining the peak temperature of the tan δ (E''/E') curve. E' (storage modulus) is a measure of the energy

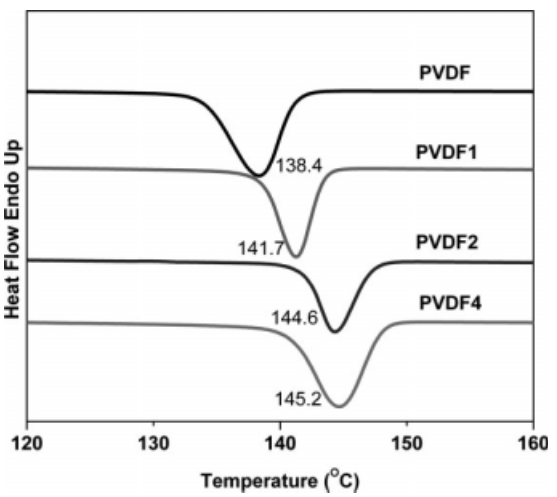

Figure 2 DSC second-cooling curves showing an increase in melt recrystallization temperatures with increasing CNF content.

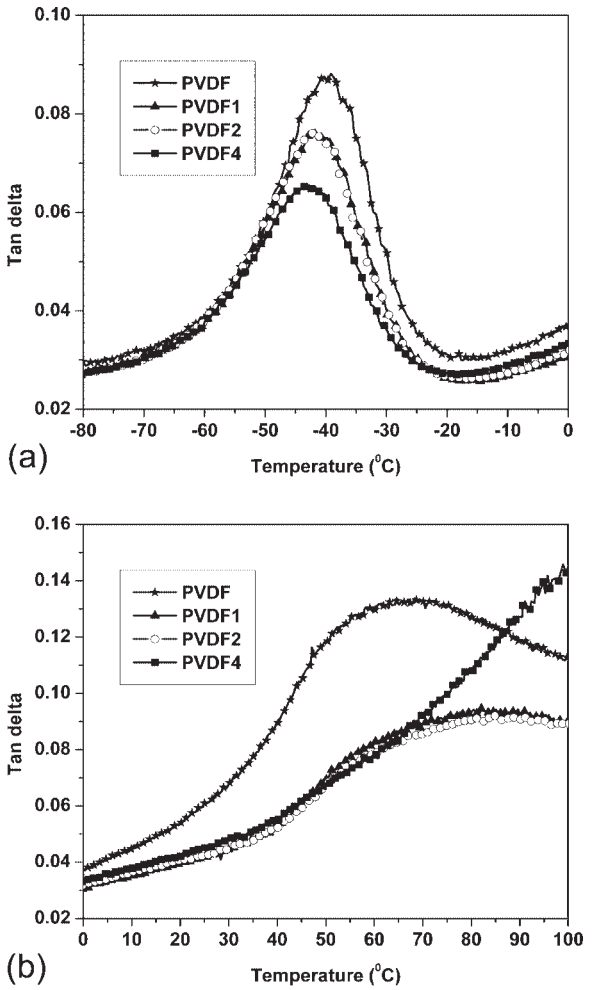

Figure 3 DMA results showing a decrease in tan δ peak height and temperature with increasing CNF content (a) for the β transition and (b) for the α transition.

stored elastically, whereas E'' (loss modulus) is a measure of the energy lost. Tan δ, also called damping, indicates how efficiently material loses energy to molecular rearrangements and internal friction. Figure 3(a) shows the β transition region of the PVDF and its composites. PVDF shows a broad β relaxation related to side chain relaxation. For PVDF1 and PVDF2, the curves overlap and indicate a slight decrease in the damping factor. A significant decrease in peak height for the PVDF4 is obtained. In addition, the β transition is shifted toward a lower temperature indicated inhibited mobility. The α relaxation region is depicted in Figure 3(b). The T_g of PVDF is 40.16°C. As can be seen, the glass transition of the composites is shifted to higher temperatures (around 80°C). We note, however, that PVDF4 does not exhibit a glass transition temperature within the range investigated and the fiber compliance prevented additional data collection. The DSC results on the decreased fractional crystallinity coupled to the increased glass transition, indicates that the improved mechanical performance in the composite is best attributed to the CNF presence.

X-Ray diffractometry

WAXD was used to observe the effect of CNF content on the microstructure of PVDF. Figure 4 shows the X-ray diffraction of PVDF and its composites. PVDF reflections are located at $2\theta = 17.8°$ (100), 18.6° (110), 19.8° (020), 26.62° (021), and 38.2° (002). These correspond to assignments for the α-phase crystal, which has nonpolar *trans*-gauche-*trans*-gauche (TGTG) conformation. We note that the composite fibers show retention of the α-phase crystal. No conversion to a β-phase is observed as indicated by an absence of a peak at an angle of about 20.6°–20.8°. The α-phase however does undergo a change with CNF presence. Two intense peaks at 17.8 and 18.6 observed in the PVDF merge into a single broad peak. We also note that the peak intensity of the (020) reflection ratioed to the (110) reflection is ~ 2 for the PVDF but drops to 1.5 in all composites. This ratio is retained when ratioing the (002) peak intensity to the (020) reflection. We therefore conclude that the transformation of crystal structure does not take place from α to β, but the nature of the α phase is affected by the presence of CNF. We predict that the crystal phase transformation did not occur

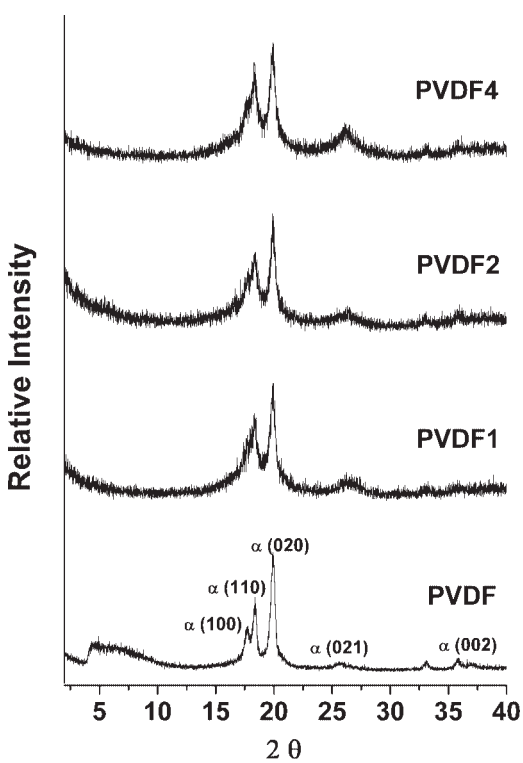

Figure 4 X-ray diffraction spectrographs for PVDF and PVDF/CNF fibers.

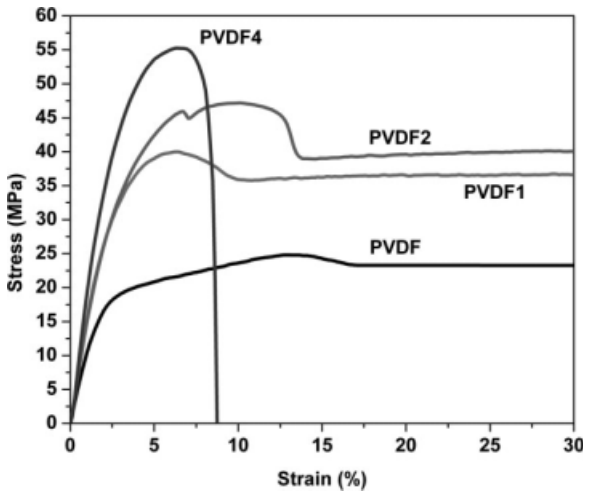

Figure 5 Stress–strain curves for PVDF and its composites.

because the extruded fibers were cold stretched and quenched in water on exit from the die.

Mechanical properties

The tensile properties for extruded fibers are shown in Figure 5. It is clear that PVDF composites offer improved tensile properties. Tensile curves were similar to those for most of the polymers. At strains past the yield, a broad plateau indicates microstructure's conversion into fibrillar morphology extensive plastic deformation for pure PVDF, PVDF1, and PVDF2. Upper yield strength and modulus values for PVDF, PVDF1, PVDF2, and PVDF4 were 25, 40, 47.5, and 55.5 MPa, respectively. A 122% increase in yield strength and an 88% increase in modulus were observed with the addition of 4 wt %. It is, therefore, not surprising that the CNFs at higher wt % loading leads to a higher yield stress. However, the elongation at break was decreased for 4 wt % CNF filler content, which can be attributed in part to modifications in the crystalline fraction in the matrix. Restriction of the amorphous phase imposed by the unidirectionally aligned nanofibers plays a key role in this behavior. The restriction sites prevent the polymer from deforming, therefore causing a decrease in ductility and an increase in stiffness. This decrease in ductility is less pronounced in both PVDF1 and PVDF2 composition, indicating a higher toughness.

Figure 6 shows the SEM images of the fractured surface of the fibers. It is clear that with increased concentration of CNF, increased fiber pullout occurs. The absence of matrix on the nanofibers coupled to pores indicating complete pullout, indicates lower interfacial adhesion between the fibers and the PVDF.

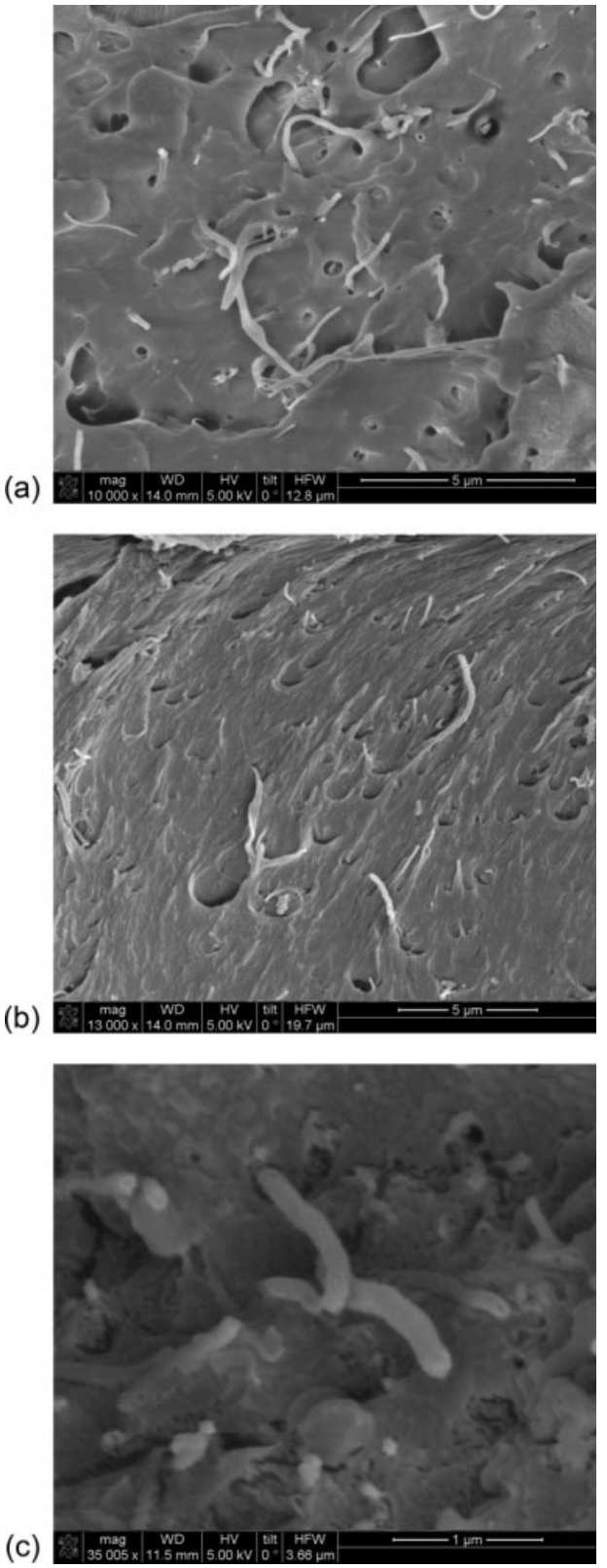

Figure 6 SEM images of PVDF composites showing fiber pull out mechanisms dominating failure (a) PVDF1, (b) PVDF2, and (c) PVDF4.

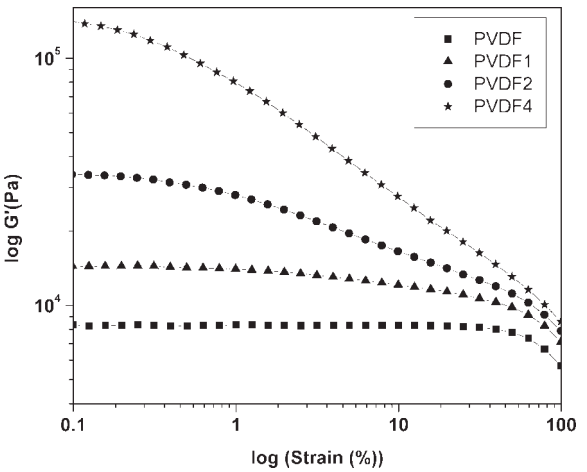

Figure 7 Dynamic strain sweep tests showing storage modulus as a function of strain.

Rheological measurements

Figure 7 shows the dependence of elastic modulus on strain at 180°C at a frequency of 1 Hz. The linear viscoelastic region for pure PVDF is very wide and up to 80% strain; but with an increase in the percentage of CNFs, the linear viscoelastic region decreases rapidly. Subsequent frequency sweeps were therefore conducted based on a constant strain of 0.1%. The elastic moduli (G'), loss moduli (G''), and complex viscosities (η^*) of PVDF and compositions are compared in Figure 8(a–c), respectively. The significant effect of CNFs can be seen, particularly at low frequency. At low frequency, PVDF/CNF composite melts have higher elastic moduli, loss moduli, and complex viscosities compared with pure PVDF and show monotonic increase with CNF content. It is conjectured that CNFs and PVDF interact and that these structures become stronger with an increase in the percentage of CNF concentration. At high frequency, however, the elastic moduli, loss moduli, and complex viscosities of PVDF and its composites are similar, indicating matrix dominance. At low frequency, a temporal structure is formed between CNFs and PVDF chains, which is strong enough to withstand the flow, resulting in the higher values of η^* at a low-frequency region. At high frequency, flow destroys some of the structure, leading to a decrease of viscosity.

CONCLUSIONS

We prepared PVDF/CNF composites by melt-blending and explored the potential of CNFs as mechanical reinforcements in PVDF composite fibers. DSC showed that CNFs decrease the fractional crystallinity in the composite. The increase in crystallization temperature with relatively no change in melting point indicates decreased supercooling in the composite. X-ray diffraction analysis indicated some change in α-phase crystallites, but β-phase transformation did not occur. A decrease in peak tan δ for

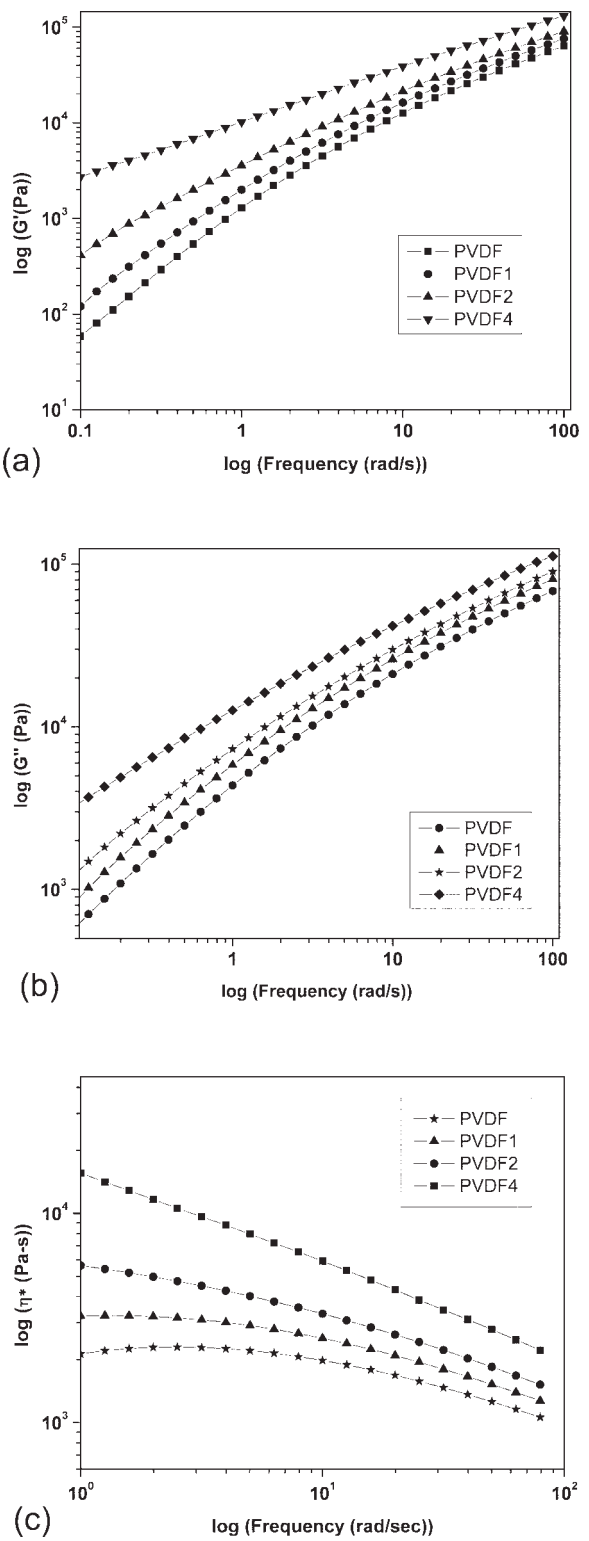

Figure 8 (a) Storage modulus G' versus frequency at 180°C temperature, (b) loss modulus, G'' versus frequency at 180°C temperature, (c) complex viscosities η^* at 180°C temperature.

both the α and β relaxation was observed. The transition temperature of the α relaxation underwent a significant increase with the presence of CNF. The increased amorphous fraction coupled to the absence of a β-phase transformation is attributed to the use of a quick quenching of the fibers in the cooling bath on exit from the extruder die. CNFs, however, were found effective in improving mechanical properties. The addition of CNFs results in an increase in ultimate tensile stress and modulus values of PVDF, suggesting that nanofibers play an important role in enhancing the mechanical properties of a polymer matrix. An increase in storage moduli, loss moduli, and melt viscosities was observed with increased CNF concentration and was significantly dependent on test frequency. We note that when 4% CNF was added to PVDF, a transition in stress–strain curves is observed together with slight increases in crystallinity. We note that higher concentrations of CNF were not processable in the extruder fiber die. This is reflected in the viscosity measurements, which show values $>10^4$ Pa s for the PVDF4 concentration.

The authors thank David Diercks, Center for Advanced Research and Technology, University of North Texas for his assistance in microscopy.

References

1. Vivek, B.; Nath, R. J Phys D: Appl Phys 2001, 34, 667.
2. Yu, X.; Rajamani, R.; Stelson, K. A.; Cui, T. Sens Actuators A 2006, 132, 626.
3. Pantelis, P. Phys Technol 1984, 15, 239.
4. Ray, H. B.; Changxing, C.; Anvar, A.; Zafar, I.; Josef, N. B.; Geoff, M. S.; Gordon, G. W.; Alberto, M.; Danilo, D. R.; Andrew, G. R.; Oliver, J.; Siegmar, R.; Miklos, K. Sci New Ser 1999, 284, 1340.
5. Gregorio, R. J. J Appl Polym Sci 2006, 100, 3272.
6. Mohammadi, B.; Yousefi, A. A.; Bellah, S. M. Polym Test 2007, 26, 42.
7. Nunes, J. S.; Sencadas, V.; Wu, A.; Kholkin, A. L.; Vilarinho, P. M.; Lanceros-Méndez, S. Mater Res Soc Symp Proc 2007, 949, 0949-C03-02.
8. Lovinger, A. J. In Developments in Crystalline Polymers; Bassett, D. C., Ed.; Applied Science Publishers: London, 1982; Chapter 5, p 62.
9. Lovinger, J. Ferroelectr Polym Sci 1983, 220, 1115.
10. Schaffner, F.; Jungnickel, B. J. IEEE Trans Dielectr Electr Insul 1994, 1–4, 553.
11. D'Souza, N. A.; Ranade, A.; Strauss, W.; Hernandez-Luna, A.; Sahu, L. In Polymer Nanocomposite Processing, Chapter 13: Handbook of Polymer Processing; Harper, C., Ed.; Wiley: New York, 2006; p 681.
12. Owens, F. J.; Jayakody, J. R. P.; Greenbaum, S. G. Compos Sci Technol 2006, 66, 1280.
13. Yu, W.; Zhao, Z.; Zheng, W.; Song, Y.; Li, B.; Long, B.; Jiang, Q. Mater Lett 2008, 62, 747.
14. Nam, Y. W.; Kim, W. N.; Cho, Y. H.; Chae, D. W.; Kim, G. H.; Hong, S. P.; Hwang, S. S.; Hong, S. M. Macromol Symp 2007, 249/250, 478.
15. Wang, M.; Shi, J.-H.; Pramoda, K. P.; Goh, S. H. Nanotechnology 2007, 18, 235701.
16. Dang, Z. M.; Fan, L. Z.; Shen, Y.; Nan, C. W. Mater Sci Eng B 2003, 103, 140.
17. Wang, L.; Dang, Z.-M. Appl Phys Lett 2005, 87, 042903.
18. Yu, X.; Rajamani, R.; Stelson, K. A.; Cui, T. Sens Actuators A 2006, 132, 626.
19. Feng, J.; Chan, C.-M. Soc Plast Eng Annu Tech Conf 1998.
20. Tibbetts, G.; Lake, M. L.; Karla, L.; Strong, K. L.; Rice, B. P. Compos Sci Technol 2007, 67, 1709.
21. Chen, G.-X.; Li, Y.; Simizu, H. Carbon, to appear.
22. Mhetre, S. K.; Kim, Y. K.; Warner, S. B.; Patra, P. K.; Katangur, P.; Dhanote, A. Mater Res Soc Symp Proc 2004, 788, L11.17.1.
23. Nakagawa, K.; Ishida, Y. Polym Sci Phys 1973, 11, 2153.